PERFORMANCE AND ECONOMIC ASSESSMENT OF A WING-INTEGRATED HYBRID LAMINAR FLOW CONTROL SYSTEM

Benjamin M.H.J. Fröhler[1], Ahmad A. Pohya[2], Jannik Häßy[3], Thomas Kilian[4], Alexander H. Bismark[5], Martin Radestock[6] & David Cruz Palacios[7]

[1]E-mail: Benjamin.Froehler@dlr.de, Phone: +49 40 2489641 316, German Aerospace Center (DLR), Institute of System Architectures in Aeronautics, Hamburg, Germany
[2]German Aerospace Center (DLR), Institute of Maintenance, Repair and Overhaul, Hamburg, Germany
[3]German Aerospace Center (DLR), Institute of Propulsion Technology, Köln, Germany
[4]German Aerospace Center (DLR), Institute of Aerodynamics and Flow Technology, Braunschweig, Germany
[5]German Aerospace Center (DLR), Institute of Flight Systems, Braunschweig, Germany
[6]German Aerospace Center (DLR), Institute of Lightweight Systems, Braunschweig, Germany
[7]Aernnova Aerospace, Madrid, Spain

Abstract

The energy efficiency of emerging aircraft designs plays a key role, not only in reducing environmental impact, but also in reducing operating costs in the anticipated rise in fuel prices. The European Clean Sky 2 project HLFC-Win is investigating the feasibility of Hybrid Laminar Flow Control (HLFC) technology integrated into the outer wing leading edge for a long-haul aircraft. HLFC technology reduces aerodynamic friction drag by means of suction of the boundary layer through a micro-perforated skin to achieve laminarity and thereby improving aircraft performance. However, integrating such a system is not without its drawbacks, as the integration has an impact on the geometry, mass, aerodynamics and engine offtakes that need to be considered. Therefore, the aim of this current work is to assess the HLFC system based on a fair, objective and transparent comparison between the HLFC aircraft and an aircraft of the same technology level without HLFC. The assessment of the HLFC system is twofold, firstly estimating the mission-based performance at the overall aircraft level and secondly performing a lifecycle simulation with three scenarios to determine realistic fuel and cost savings. The mission-based performance assessment indicates a block fuel reduction of over 3 % for the design mission which averages 1.6 to 2.5 % considering a realistic route scenario and expected degradation. The economic assessment suggests a dependency on the scenario chosen, ranging from a 0.7 % increase in total cost (in an unfavourable scenario) to almost a 1 % reduction in total cost (in a favourable scenario), equivalent to $15 million saved per HLFC aircraft over its lifetime. These results support the commercial viability of HLFC technology, which offers significant aerodynamic and fuel efficiency improvements and operating cost savings to the aviation industry. Importantly, no critical barriers were identified for the integration of HLFC technology, further underscoring its potential to improve aircraft performance.

Keywords: Hybrid Laminar Flow Control, Overall Aircraft Performance, Life Cycle Simulation

1 Introduction

The aviation industry's commitment to energy efficiency is imperative, given its significant contribution to greenhouse gas emissions and the expected rise in fuel prices. Improving energy efficiency not only aligns with global environmental goals, but also strategically prepares the industry for economic resilience and long-term sustainability. Prioritizing fuel-efficient technologies and practices is critical to reducing the sector's environmental impact and ensuring operational viability in a resource constrained world.

Therefore, the European Commission already formulated Europe's Vision for Aviation in the ACARE Flightpath 2050 to lower the fuel consumption and emissions of aircraft [1]. The Clean Sky 2 Joint

Undertaking (CS2JU) is an initiative within the framework of the Flightpath 2050. CS2JU focuses on the investigation and the development of the mostly promising technologies. One of these technologies is hybrid laminar flow control (HLFC). This technology has been well studied since the late 1980s and good overviews are given by Collier and Joslin [2, 3]. The application since then also includes application of HLFC on aircraft such as the JetStar wing [4, 5], the wing of a Boeing 757 [6, 7] or the A320 fin [8, 9, 10]. The test setups were often very heavy and focus on aerodynamic studies to achieve a benefit in drag reduction. Instead, the HLFC-Win project focuses on the application of HLFC technology on a wing with all relevant disciplines. The combination of aerodynamics, structures and systems allows the maturation of the technology for an integrated system within a realistic leading edge. Such a development enables the assessment on aircraft level and allows an improved quantification of the block fuel reduction in relation to additional masses and engine offtakes.

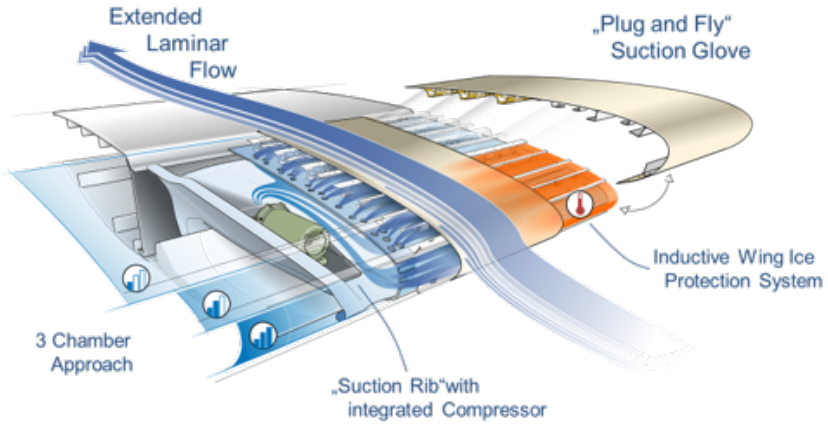

Figure 1 – Integration of a HLFC system into an outer wing leading edge [11, 12].

This paper is structured as follows: after the introduction, the methodology used is presented in Chapter 2, including the performance assessment in Chapter 2.1 and the lifecycle assessment in Chapter 2.2 . Chapter 3 provides a detailed discussion of the aircraft configurations, including descriptions of the reference and baseline aircraft and insights into the integrated HLFC aircraft configuration. Chapter 4 then presents a comparative analysis between the baseline and HLFC aircraft, detailing the results obtained. A conclusion summarising the key design decisions and outlining possible directions for future developments for further research is provided in Chapter 5.

2 Assessment Methodology

For a holistic assessment of a HLFC system, not only the effects on the aircraft performance but also the economic effects have to be considered. Therefore, two methods have been applied, the first focused on the aircraft itself and the second considering its service life.

2.1 Performance Assessment

In the field of aircraft conceptual design and the incorporation of new technologies, the use of an Aircraft Design Environment (ADE) is essential to provide a comprehensive representation of the aircraft. In this study, the ADE developed by Fröhler et al. [13], specifically tailored for the project, is used and its functionality is extended to include the HLFC system. The capabilities of the ADE, shown in Figure 2, include the assessment of aircraft performance and the facilitation of a seamlessly cohesive aircraft design. A workflow-driven integration platform, the Remote Component Environment (RCE) [14, 15, 16], is used to synergize the various tools at both the conceptual aircraft design and higher-fidelity disciplinary levels. Within this multidisciplinary ADE framework, sub-processes communicate through a standardized language, facilitated by the DLR's standardized data schema CPACS [17], ensuring efficient information exchange and storage of aircraft characteristics data. The result of this design process is a detailed aircraft description, covering key aspects such as geometry, aerodynamics, mass properties, engine specifications and overall aircraft performance. For the assessment of the HLFC system, a key enhancement has been the extension of the aerodynamic tools to include

methodologies related to laminar flow technologies. This enhancement becomes integral to the estimation of the aircraft's mission performance, ensuring a comprehensive evaluation that encompasses the impact of the HLFC system on the overall performance metrics.

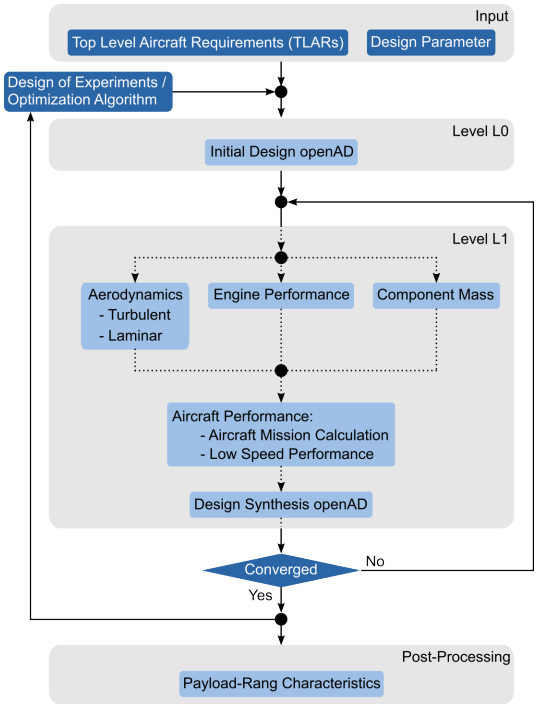

Figure 2 – Illustration of the aircraft design process [13].

A more detailed analysis of the mission performance is required for the subsequent lifecycle assessment of the HLFC system. For this purpose, the DLR internal software AMC (Aircraft Mission Calculator) [18, 19] is used to calculate the payload-range characteristics of the analyzed aircraft. The AMC software uses fuel fractions for the taxiing, take-off, and approach & landing phases and estimates the climb, cruise and descent performance by solving the 2D equation of motion with a clean wing configuration, i.e. the control surfaces are retracted. An optimization of the initial cruise altitude is performed and during the cruise phase a combination of constant altitude and step climbs in between is applied. These step climbs are initiated automatically, depending on the specific range, considering the aircraft's aerodynamic and engine performance.
To simulate the life of an aircraft, the process manipulates the aircraft mass, aerodynamics and engine performance to account for the ageing of an aircraft in the later lifecycle simulation. The Mach number can also be manipulated to simulate different operating conditions. The limits of the payload range diagram are then calculated using the AMC software. This provides the outer boundaries which are used to generate additional samples with different combinations of payload and range. The additional samples are again calculated using the AMC software. Finally, a surrogate model for the lifecycle evaluation is generated on the basis of these results.

2.2 Lifecycle Assessment

The lifecycle-based assessment is performed with the simulation framework called LYFE (LifecYcle cash Flow Environment) [20]. It uses a discrete event simulation with variable time increments to model the entire life of an aircraft or fleet, from their order until their disposal. These discrete events include the order, delivery, all flight and maintenance events, and the sale or disposal of the aircraft. Each event holds attributes such as the start time and duration, as well as cost and revenues (if applicable). For a flight event, for example, the cost elements include the landing and navigation fees, airport handling charges, crew cost, and fuel cost. Each of these is calculated using either regression-based cost estimation relationships (as used in Direct Operating Cost (DOC) estimation methods) or more sophisticated approaches (e.g. machine learning models trained on cost databases).

This work examines the operator's perspective to determine the economic superiority of the HLFC aircraft over a conventional and turbulent alternative. To do so, at least two executions of the simulation are needed: one for the baseline and one for the HLFC aircraft. For a proper evaluation, a total of six simulations were analyzed. These represent three different scenarios for each aircraft and aim to address top-level uncertainties such as the future fuel price. In addition, the low-level uncertainties have been treated with probabilistic measures. The next chapter describes the inputs, assumptions, and uncertainties in more detail.

2.2.1 Design Assumptions

In this section, the assumptions for the input data are described in more detail and are categorized as general, operation, and maintenance assumptions. If not mentioned otherwise, the inputs are identical for both the baseline and HLFC aircraft configurations.

General The input data in the general category are:

- The entry into service date is 01.01.2030 and both aircraft are operated for 20 years.
- Both aircraft are sold at the end of their operational life for a residual value of 10 %.
- Both aircraft are bought, i.e. not leased, by the operator. The financing structure is based on Clark [21].
- The base year for the assessment is 2023, i.e. all monetary values are expressed in USD for the year 2023.
- The HLFC system is activated during cruise, only.
- The HLFC system requires annual maintenance but does not need to be replaced during the 20 years of operational life.

Operation The operational schedule is shown in Figure 3. This route network is based on an analysis of Lufthansa's A330-343 fleet as of the year 2020. As the network shows, the aircraft are based in Frankfurt (FRA), Germany and fly to destinations in the USA, Africa, the Middle East, and a few in West Asia. This schedule is flown randomly while respecting the relative frequencies of each origin and destination pair, which leads to a realistic distribution of flown missions throughout the lifecycle. The average distance and average flight time are 3410 NM and 7:45hrs, respectively. This results in about 657 flight cycles per year, which is relatively close to the actual operation of most of Lufthansa's A330-343. Note that the payload (incl. passengers) is treated as an uncertainty and hence described later (see Chapter 2.2.2). Furthermore, it is assumed that the aircraft only carry passengers, i.e. the airline's operational revenue stream comes only from sold fares as well as ancillary revenues.
As for the HLFC aircraft, it is assumed that the airline carries an extra amount of contingency fuel for cases of unforeseen losses of laminarity. The amount of carried contingency fuel is treated as an uncertainty and is also described later. Note that the additionally carried mass affects the fuel performance of the HLFC aircraft negatively, but allows for a more realistic assessment.

Maintenance For the maintenance schedule, it is assumed that the operator uses the maintenance plan of the Airbus A330, which consists of line maintenance (transit-checks, daily-checks, and weekly-checks), base maintenance (A-checks and C-checks with a repeating pattern of 8 years), and heavy component maintenance (e.g. for tires, landing gear, thrust-reversers, as well as engine shop visits). This maintenance schedule is summarized in Table 1 alongside the cost and assumed downtime. These maintenance events are automatically triggered by the simulation and contribute to a more realistic assessment – despite being identical for both aircraft designs and ultimately cancelling each other out when calculating the Δ values. Unscheduled maintenance is calculated as a time-dependent function where the ratio of unscheduled maintenance cost to scheduled maintenance cost varies from 1.0 (in the first operational year) to 1.75 (in the last operational year), according to Suwondo [22].
As for the HLFC maintenance, only an estimation of the expected cost can be given at this point due to the lack of operational data (e.g. frequency of clogged surfaces or average/standard deviation

of compressor failures). To account for the uncertainty in the estimation of the HLFC maintenance, experts from the advisory board have been interviewed. More information follows in the next chapter.

Table 1 – Used maintenance schedule, based on data from Aircraft Commerce articles [23, 24] for the Airbus A330.

Name	Type[1]	Downtime	Interval	Fiscal year	Total cost
Transit	L	0.5	Between each flight	2008	$120
Daily	L	1	Every Day	2008	$330
Weekly	L	2	Every Week	2008	$920
A1-A8	B	7-10	Multiples of 800 FH	2008	$36k to $50k
C1-C8	B	70-720	Multiples of 1.5 years	2008	$215k to $2.2M
Various components	H	2-10	After specific FC counter	2008	$1k to $900k
ESV's	H	6	FH or FC triggered	2012	$4M to $6M

[1] L: line maintenance, B: base maintenance, H: heavy component maintenance

2.2.2 Uncertainties

As is common in prospective assessments of aircraft and technologies at this stage of the development, uncertainties are inevitable and should be considered and quantified where possible. When data for uncertainty quantification (UQ) are available, probabilistic techniques such as probability density function (PDF) fitting and subsequent quasi-random sampling are employed. If data are scarce or entirely unavailable, subject matter experts (SMEs) have been interviewed in order to utilize their knowledge. Both approaches are described below.

TSFC Penalty during HLFC operation To operate, the HLFC system requires electrical energy, which is drawn from the engine generators during cruise. This introduces a Thrust Specific Fuel Consumption (TSFC) penalty, which has to be outweighed by the gains in drag reduction for a successful HLFC aircraft. The quantification of said TSFC penalty depends on a variety of factors, out of which the electrical efficiencies of the components play a major role. The basis for this quantification is the suction power P_{suc}, for which an aerodynamic analysis was conducted. In this analysis, the Flight Level (FL), cruise Mach number (Ma), and lift coefficient C_L have been varied and the suction power has been computed for each combination. Table 2 shows an excerpt for Ma = 0.83, out of which

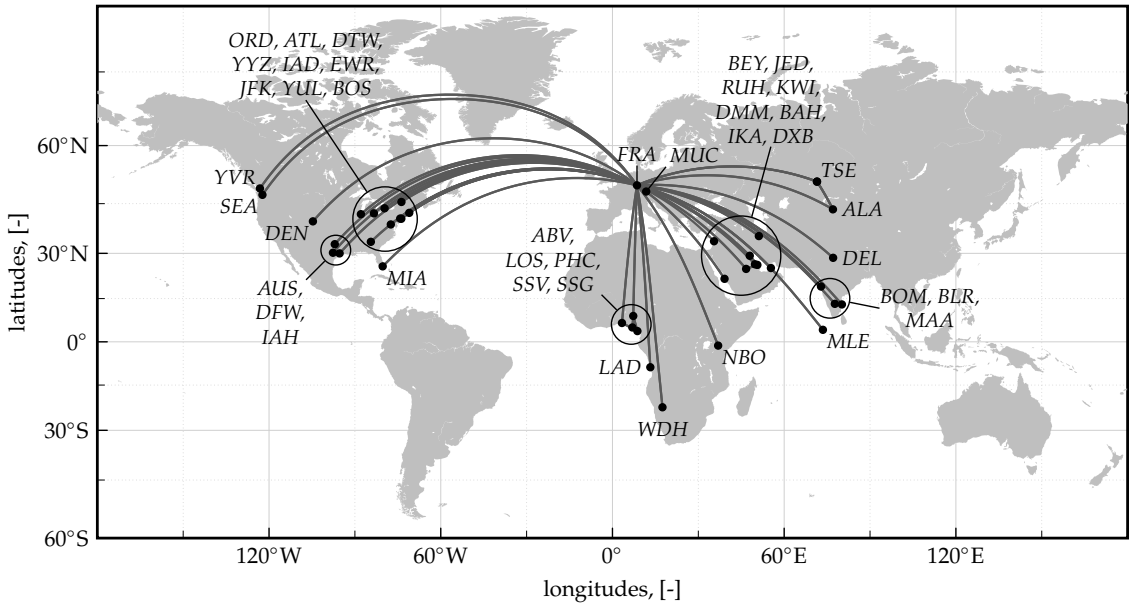

Figure 3 – Route network, based on Lufthansa's A330-343 fleet as of 2020, depicted as great circles.

an average suction power of 48 kW was obtained[2]. The same approach was taken for the other two cruise Mach numbers 0.81 and 0.83, for which the average suction powers are 56 kW and 49 kW, respectively. This averaging was needed due to the way the engine performance decks are created, out of which the fuel performance is calculated during the mission simulation in AMC.

Table 2 – Excerpt of the aerodynamic analysis for the estimation of the suction power per half wing for Ma = 0.83.

	FL330	**FL360**	**FL390**	**FL420***
$C_L = 0.45$	53 kW	49 kW	43 kW	38 kW
$C_L = 0.50$	53 kW	54 kW	48 kW	47 kW
$C_L = 0.55$	55 kW	62 kW	50 kW	51 kW

* FL430 was extrapolated using linear regression due to missing data

To incorporate the uncertainty, the expected electrical efficiencies of the compressors, inverters, generators, and powerlines are used. Based on data from a compressor feasibility study as well as publicly available information for the remaining components [25], the overall suction system efficiency uncertainty is

$$\eta_{\text{suc}} \sim \mathscr{U}(0.424, 0.455) \quad . \tag{1}$$

With this, the shaft power offtakes (i.e. those drawn from the generator) can be calculated using

$$P_{\text{HLFC}}(Ma) = \frac{P_{\text{suc}}(Ma)}{\eta_{\text{suc}}} \quad . \tag{2}$$

Table 3 shows the ranges of shaft-power offtakes considering the uncertainties in the electrical efficiencies. These have then been translated to TSFC penalties using literature values for an engine suitable for the Airbus A330, with the range from 0.5 to 0.7 % per 100 kW [26]. These represent the final ranges that are implemented in the lifecycle-based performance assessment. More specifically, the "Min" column of the TSFC penalty is used to interpolate from the so-called "advantageous" scenario. In the same manner, the "Mean" and "Max" columns are used for the "intermediate" and "disadvantageous" scenarios respectively.

Table 3 – Cruise Mach specific shaft-power offtakes.

Operating Condition		**Shaft-Power Offtakes [kW]**			**TSFC Penalty [%]**		
FL	**Ma**	**Mean**	**Min**	**Max**	**Mean**	**Min**	**Max**
330-430	0.81	127	123	132	0.763	0.614	0.922
330-430	0.83	110	106	114	0.658	0.529	0.795
330-430	0.85	113	109	117	0.676	0.543	0.817

Mach Number during Cruise and its Effect on the Laminar Efficacy The cruise Mach number affects the laminarity of the HLFC aircraft and consequently its fuel efficiency. To integrate it in the assessment, two steps needed to be performed. The first step was to determine the variations in real cruising speed. Secondly, the effect of this variation on the laminarity had to be quantified. For the first step, representative flight trajectories of Airbus A330-300 aircraft from FlightRadar24 [27] were analysed. As these only provide the current time, altitude, latitude, and longitude (and hence its ground speed) of an aircraft, the cruise Mach number is not readily accessible. Therefore, these trajectories were coupled with the weather database from the ECMWF [28] to calculate the present wind speed, temperature, pressure, and speed of sound that the aircraft experiences. The resulting Mach number histogram is depicted in grey in Figure 4 (top left). From this distribution, it can be observed that the A330 flies with an average speed close to its design cruise Mach number of 0.82. Since the XRF1 as well as the HLFC aircraft have a design Mach number of 0.83, this distribution has been shifted by +0.01 (see blue histogram).

[2] As it will be discussed later, the aircraft's lift coefficient during cruise stays mostly in the interval [0.45,0.50], which is why the row with C_L=0.55 was ignored for these analyses.

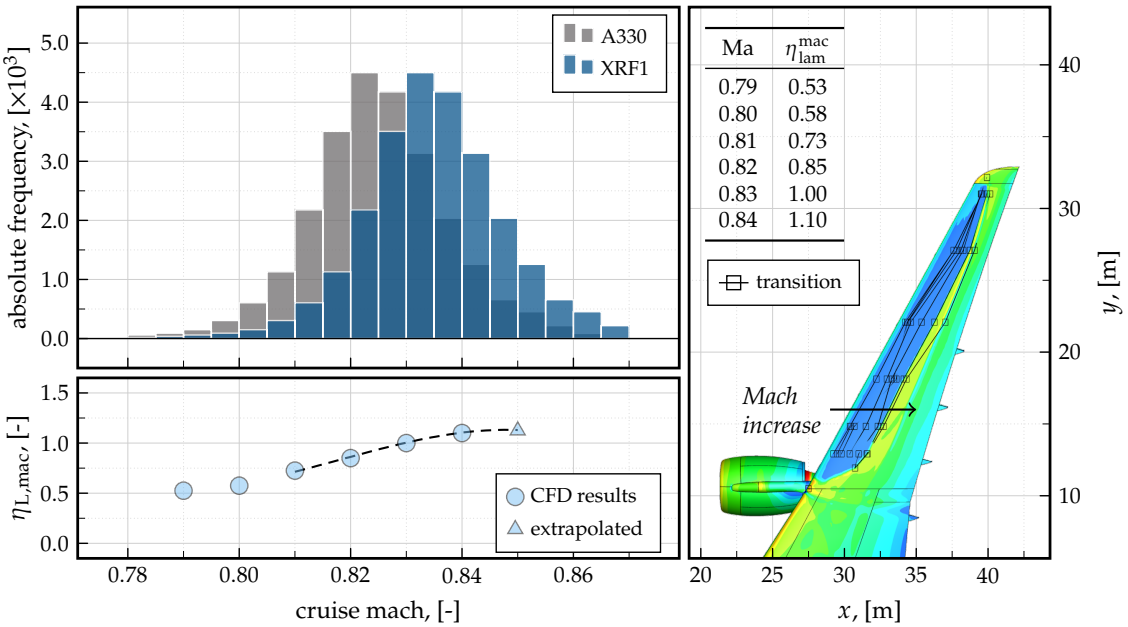

Figure 4 – Histogram of calculated cruise Mach number of an Airbus A330-343 (top left), high-fidelity CFD results with laminar efficacy values (compared to itself when turbulent), colour coded by the skin friction coefficient (right), and the regression model obtained from it (bottom left) [25].

For the second step, i.e. the effect of different cruise speeds on laminarity, the results of a high-fidelity CFD simulation of the configuration were used. Here, cruise Mach number have been varied and the impact on the transition and drag reduction potential was calculated. The right plot in Figure 4 illustrates the spanwise transition, whereas the bottom left plot depicts the results of the Mach number variation on the laminar efficacy. For this, the drag reduction at Ma = 0.83 was normalized to 100 %. As the data shows, lower Mach numbers result in a significant loss of laminar efficacy, whereas higher speeds seem to be favourable. For more information on this parameter, consider Pohya [25].
In the lifecycle simulation, one cruise Mach number is sampled according to the aforementioned distribution before each flight. Both aircraft fly to their destination with this cruise speed. To quantify the impact of the laminar efficacy on the fuel performance, the degradation due to cloud encounter (described next) is needed.

Time in Cloud The degradation of laminarity due to cloud encounter at high altitudes has been proven in various flight tests. For this analysis, the statistics of the relative time in cloud t_c obtained from flight test data were used. Before each simulated flight, one value for t_c is sampled according to the distribution shown in the top of Figure 5 and then translated using the linear regression model depicted at the bottom. This results in an overall laminar efficacy of

$$\eta_L = \eta_{L,\text{mach}} \cdot \eta_{L,\text{cloud}} \quad . \tag{3}$$

The fuel performance of the HLFC aircraft is then calculated using an interpolation between the laminar and non-laminar aerodynamic performance map, where η_L is used as the interpolation coefficient.

Passenger load factor The number of passengers carried varies with the airline, route, season, and other factors. For this project, published data from the US Department of Transportation (DoT) [29] has been used, which averages to about 80 %. Before each flight, a passenger load factor is sampled according to the distribution shown in Figure 6. Both aircraft then fly their route with the same passenger load factor.

Carried Contingency Fuel for the HLFC system Operators of HLFC aircraft may wish to include some additional contingency fuel $m_{\text{fuel,cont}}$ to account for unforeseeable losses of laminarity, e.g. due

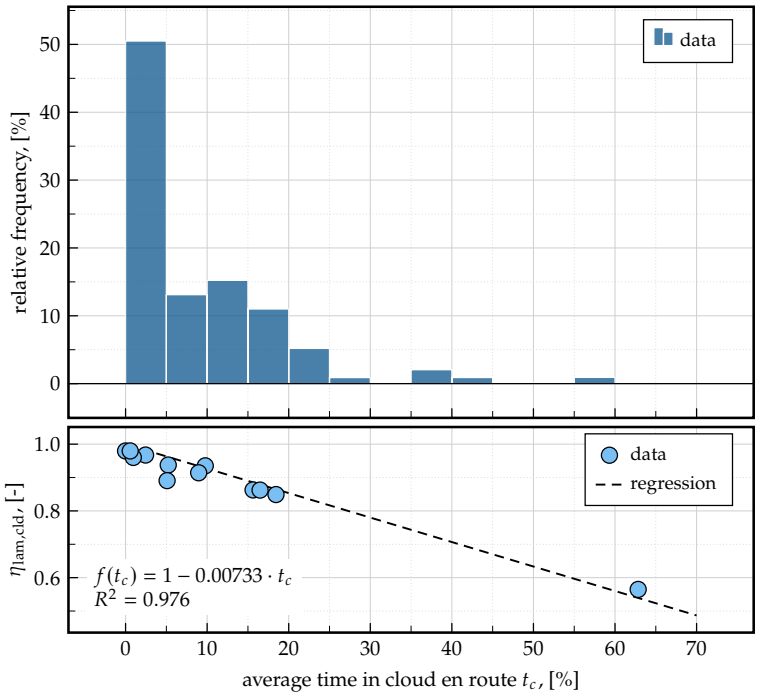

Figure 5 – Histogram of average time in cloud en route (top) and its impact on the laminar efficacy (bottom) [25].

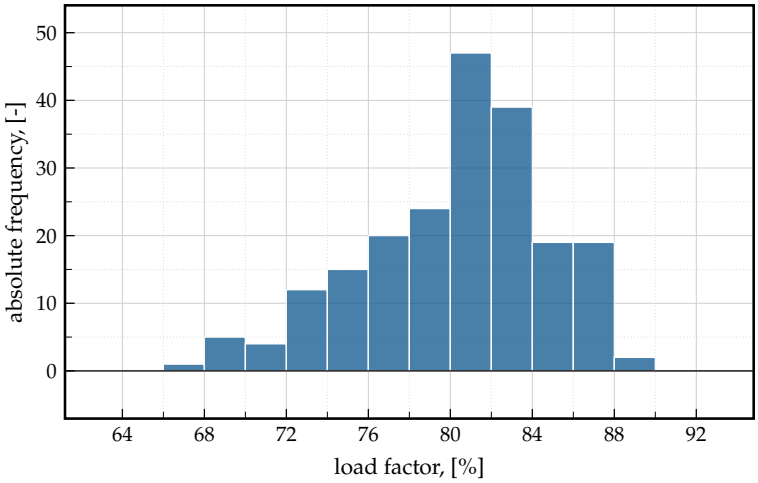

Figure 6 – Histogram of average load factors based on data between 2002 and 2019 from the US DoT [29]

to an unexpectedly high time in cloud or failures of components. Depending on the operators' preferences, this contingency can range from zero (risk-tolerant) to a maximum (risk-averse). The latter is likely to be equal to the amount of fuel that the HLFC system would save on the given route. To model this uncertainty, an interpolant c_{int} between these two extreme values is introduced and varied uniformly from 0 to 1, i.e.:

$$m_{\text{fuel,cont}} = c_{\text{int}} \cdot (m_{\text{fuel,turb}} - m_{\text{fuel,lami}}) \quad \text{with} \quad c_{\text{int}} \in [0, 1] \tag{4}$$

Here, $m_{\text{fuel,turb}}$ refers to the planned block fuel of the HLFC aircraft if the HLFC system is turned on but does not work, e.g. because it is fully contaminated. $m_{\text{fuel,lami}}$ refers to the block fuel of the HLFC aircraft if there is no loss of laminarity. Because this uncertainty is more of an airline specific value, rather than something that is decided anew day to day, c_{int} is *not* sampled before each flight like the previous uncertain parameters. Instead the aforementioned scenarios are used, where a value is fixed for each lifecycle simulation:

1. **disadvantageous**: $c_{\text{int}} = 1.0 \Rightarrow m_{\text{fuel,cont}} = m_{\text{fuel,turb}} - m_{\text{fuel,lami}}$. This means that the operator always carries an amount of contingency fuel that is equal to the maximum savings of the HLFC system. This in turn reduces the overall fuel efficiency due to the additional mass.
2. **neutral**: $c_{\text{int}} = 0.5$. Here, the operator carries half of the maximum savings.
3. **advantageous**: $c_{\text{int}} = 0.0 \Rightarrow m_{\text{fuel,cont}} = 0$. Here, no additional contingency fuel is carried. Thus, the operator assumes that the generally carried contingency fuels are sufficient for any expected losses.

Note that $m_{\text{fuel,cont}}$ is treated as a generic added mass in the simulation. There is no advanced en-route fuel planning algorithm implemented.

Future Fuel Price The price per unit of fuel is known to vary greatly and predictions of the future fuel price development are naturally uncertain. The US Department of Transportation therefore uses multiple scenarios in their annual energy outlook (AEO) [30] considering various market assumptions. Figure 7 shows the so-called “reference” case as well as two boundary case scenarios named "low oil price" and "high oil price" provided by the AEO alongside the historic development. These fuel price progressions are therefore used for the lifecycle simulation:

1. **disadvantageous**: Ranging from 0.52 USD/kg (1.60 USD/gal) in 2030 to 0.58 USD/kg (1.77 USD/gal) in 2050.
2. **neutral**: Ranging from 0.90 USD/kg (2.77 USD/gal) in 2030 to 1.01 USD/kg (3.10 USD/gal) in 2050.
3. **advantageous**: Ranging from 1.57 USD/kg (4.82 USD/gal) in 2030 to 1.79 USD/kg (5.49 USD/gal) in 2050.

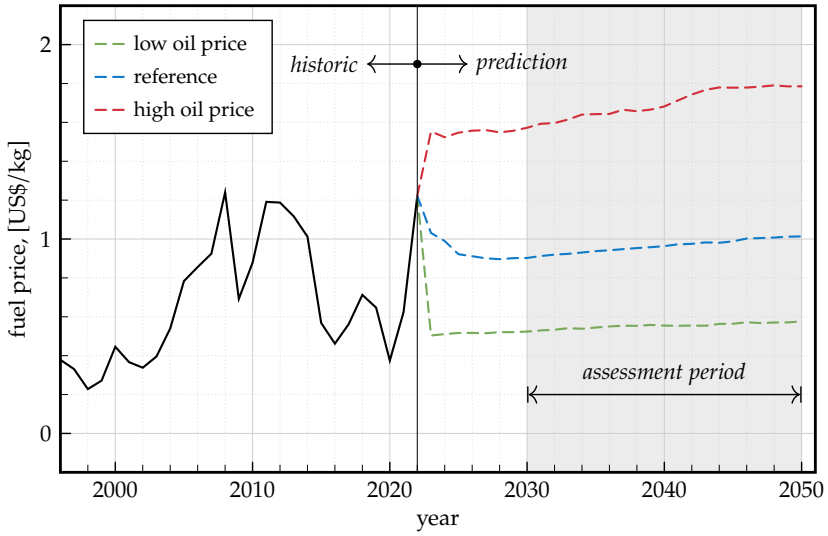

Figure 7 – Historic and projected kerosene price with low, reference, and high oil price scenarios (taken from the US Energy Information Administration [30]).

Uncertainties without Plentiful Data As opposed to the previously described uncertain parameters, there is little to no reliable data for estimating the increase in maintenance cost and aircraft price. These are therefore modelled with a new approach that is based on evidence theory. For this approach, SMEs have been interviewed and asked to provide so-called "Belief" values for intervals in which the value of interest may lie in. In other words, the experts’ belief in the parameter is elicited

and used to create a distribution of potential values. More information on this approach can be found in Pohya [31].
The two uncertainties treated with evidence theory are the increase in maintenance cost and aircraft price due to the introduction of the HLFC system. The maintenance cost increase has two parts: (a) The scheduled portion, which is given in USD per Flight Hour (USD/FH) units, and (b) the ratio of unscheduled to scheduled HLFC maintenance cost, given as a percentage-value. The aircraft price increase is defined in USD/kg. For each element, three SMEs have provided intervals and beliefs, which are shown in the top part of Figure 8. Each pattern represents one SME, the box width represents the interval and the height represents the belief in this interval. If the height of a box is high, there is high belief that the true value of the parameter lies within there, which results in more samples being drawn from this interval. The according sample space is shown in the bottom part of the figure.
All three of these elements are assumed to be fixed for one lifecycle simulation, i.e. they are not assumed to vary from year to year within a lifecycle. Therefore, we follow the scenario approach outlined before, defining these three cases:

1. **Advantageous**: The scheduled maintenance cost is assumed to be 5 USD/FH. The unscheduled maintenance cost is assumed to be 100 % of the maintenance cost, adding another 5 USD/FH, which results in total HLFC maintenance cost of 10 USD/FH. The cost of HLFC is assumed to be 1410 USD/kg, whereby the kg value represents the mass difference between the HLFC aircraft and the baseline. As will be discussed later, this mass difference computes to 1330 kg, resulting in an aircraft price increase of 1.9 million USD.

2. **Neutral**: The scheduled maintenance cost is assumed to be 8 USD/FH. The unscheduled maintenance cost ratio is 140 %, adding 11 USD/FH, which results in total maintenance cost of 19 USD/FH. The HLFC cost is assumed to be 1750 USD/kg, resulting in an aircraft price increase of 2.3 million USD.

3. **Disadvantageous**: Here, the scheduled maintenance cost is 10 USD/FH and the unscheduled ratio is 180 %, adding 18.5 USD/FH, resulting in total HLFC maintenance cost of 29 USD/FH. The HLFC cost is 2053 USD/kg, resulting in an aircraft price of 2.7 million USD.

These values have been defined using the lower third, centre, and upper third of the intervals of Figure 8 using the 0^{th}, 33^{rd}, 66^{th}, and 100^{th} percentile of the sample space, resulting in a weighted and more representative split. Within these thirds, the average value was used for the scenario values.

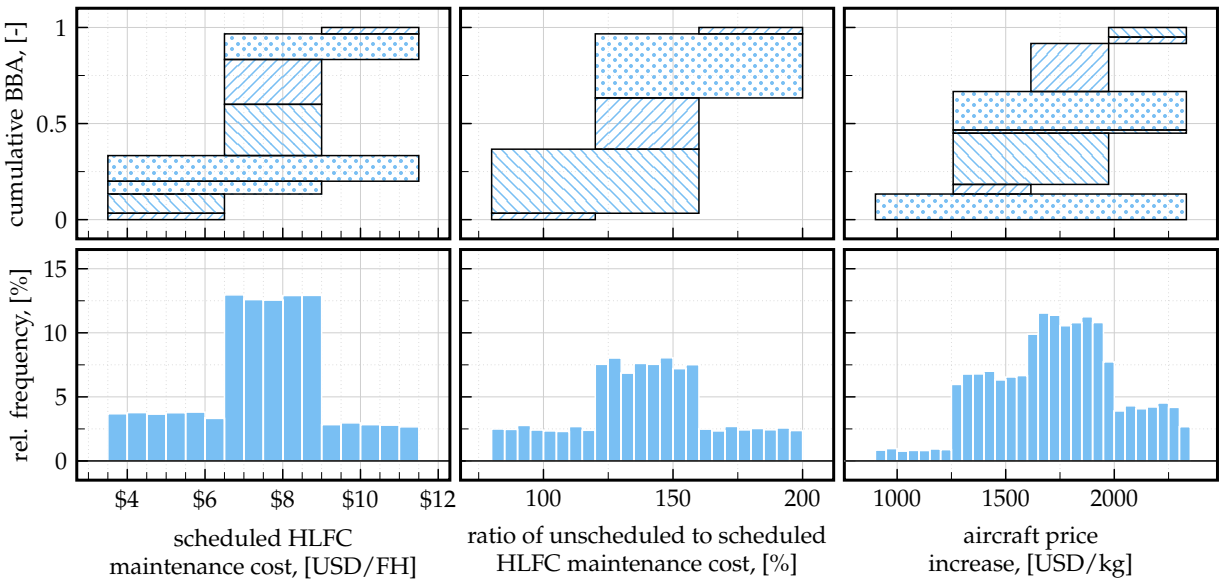

Figure 8 – Increase in maintenance cost and aircraft price, treated with Evidence Theory

3 Aircraft Configurations

To assess the impact of disruptive technologies such as the HLFC system, it is imperative to establish an evolutionary baseline aircraft for comparison. This baseline serves as a common technology benchmark that reflects the state of the art within a specified time frame. The initial phase involves the selection of a reference aircraft that meets the Top-Level Aircraft Requirements (TLARs) and provides a comprehensive set of established values essential for method calibration. The evolutionary baseline aircraft is then created to ensure comparability at an equivalent level of technology. Subsequently, the integration of the HLFC system can be methodically introduced in incremental steps.

3.1 Reference Aircraft

The reference aircraft chosen for this project is the AIRBUS XRF1, which was selected because it provides a consistent data set and meets the TLARs. The publication by Fröhler et al. [13] describes the AIRBUS XRF1 in detail and provides a comprehensive description of all relevant data. For the DLR redesign, the conceptual aircraft design tool openAD [18, 13] was used as described in Chapter 2.1, following the DLR internal project VicToria [32] and the project Con.Move: Nekon [33] of the German Aerospace Research Program (LuFo). Table 4 lists the TLARs associated with the reference aircraft. For the mission analysis, two ranges are considered: the design mission and a study mission covering ranges of 5500 NM and 3000 NM, respectively. The design mission, used for sizing the aircraft at maximum take-off mass (MTOM), requires a payload of 31.5 t, consisting of 300 passengers at 105 kg each. Conversely, the study mission assumes a payload of 25.2 t. The aircraft's operational parameters include a design cruise Mach number of 0.83, an initial cruise altitude (ICA) of 33 000 ft, and a ceiling altitude of 43 000 ft for both missions. In addition, the aircraft is designed to meet an airport compatibility limit of ICAO Code E, with an approach speed in accordance with ICAO Category C.

Table 4 – Top-Level Aircraft Requirements of the reference aircraft [13].

Parameter	Unit	Value
Technology Status Airframe	Year	1995
Technology Status Wing and Engine	Year	2010
Design Range	NM	5500
Study Mission Range	NM	3000
Design Cruise Mach Number	-	0.83
Initial Cruise Altitude	ft	33000
Service Ceiling	ft	43000
Take-Off Balanced Field Length (SL, ISA)	m	$\leqslant$2800
Landing Field Length (MLM, SL, ISA, Dry RWY)	m	$\leqslant$2250
Max. operating Mach number (MMO)	-	0.87
Max. operating speed (V_{MO})	kn	340
Climb Speed (Calibrated Airspeed)	kn	300
Descent Speed (Calibrated Airspeed)	kn	250
Approach Speed Category	-	ICAO Category C
Number of Passengers (3 Class Standard Layout)	-	300
Design Mission Payload (105 kg/PAX)	t	31.5
Study Mission Payload (105 kg/PAX)	t	25.2
Max Payload	t	48
ICAO Aerodrome Reference Code	-	ICAO Code E

The three-view representation of the reference aircraft shown in Figure 9 is derived from the AIRBUS XRF1 research configuration and integrated into CPACS through the conceptual aircraft design tool openAD, using a simplified geometry for compatibility. Although the simplification is necessary to adapt the input to openAD, it does not compromise the fidelity of the aerodynamic calculations, as the aerodynamics in openAD are calibrated based on high-fidelity calculations and the detailed CAD geometry. The wing configuration adheres to the jig shape and represents a five-station wing without

winglets, resulting in a reference area of 374.55 m^2 and a span of 58 m. The volume coefficient of the vertical and horizontal tail planes is determined by their reference areas and the respective lever arms of the tail. Clearance angles are estimated, with the rear and side clearance angles of 10.7° and 11°, respectively, exceeding the minimum required clearance.

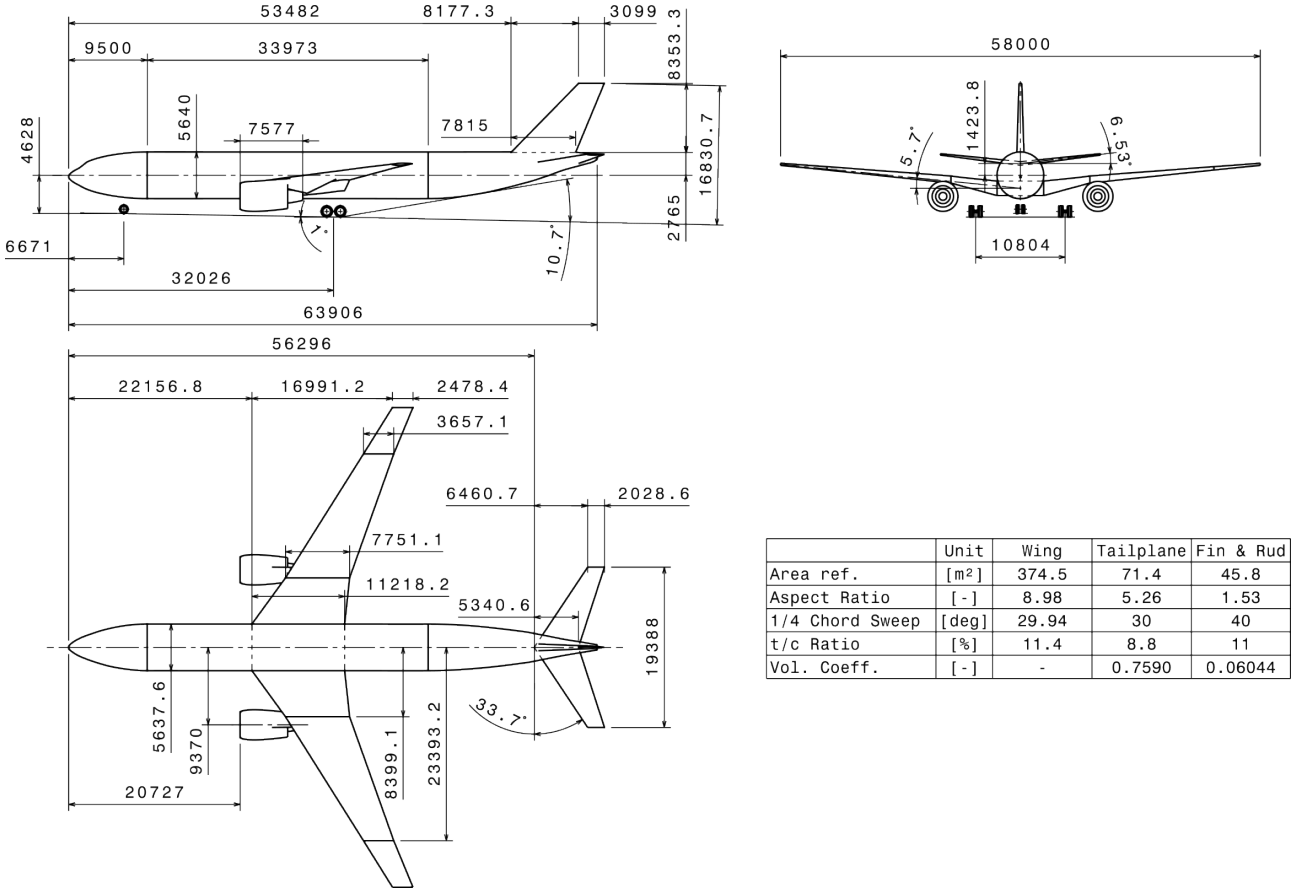

	Unit	Wing	Tailplane	Fin & Rud
Area ref.	[m²]	374.5	71.4	45.8
Aspect Ratio	[-]	8.98	5.26	1.53
1/4 Chord Sweep	[deg]	29.94	30	40
t/c Ratio	[%]	11.4	8.8	11
Vol. Coeff.	[-]	-	0.7590	0.06044

Figure 9 – Three-View of the reference aircraft [13].

3.2 Baseline Aircraft

The baseline aircraft follows the same TLARs as the reference model. To accurately assess the impact of a new technology, such as the HLFC system, the aircraft must be projected to its anticipated entry into service (EIS) year, when the technology is expected to be commercially available. Therefore, the baseline aircraft is assumed to reach EIS in 2030, incorporating advances in airframe structure and material technologies, propulsion systems, and aerodynamics. Differences between the reference and baseline aircraft are primarily due to variations in airfoil and wing planform, related to the projection into a future technology scenario. Table 5 lists the technology factors applied to the reference aircraft, supplemented by changes in wing planform. For the baseline aircraft, a more detailed assessment of the aerodynamics (see Streit et al. [34]) resulted in a cruise lift over drag ratio (L/D) of 20.5. Adopting a 1g-flight shape resulted in a half span of 28.85 m, with aerodynamic coefficients derived from Streit et al. [34]. In addition, incremental technological improvements were incorporated for the year 2030, including the use of new materials to reduce structural mass and the development of an optimized engine design. Of note are the expert assumptions for mass reduction in the wing, fuselage, and tail structures due to advances in manufacturing, assembly methods, and improved material properties. The gas turbine undergoes significant changes, moving from a 3-spool to a geared turbofan architecture, resulting in a 17 % increase in mass. At the same time, engine performance is improved by raising the temperature and pressure levels in the thermodynamic cycle, optimizing component efficiency, and slightly adjusting the bypass ratio while keeping the engine diameter constant.

Table 5 – Technology factors for an assumed technology scenario in the year 2030 of the Baseline aircraft.

Component	Technology Factor	Description
Wing Structure Fuselage Structure Empennage Structure	–15 % –10 % –20 %	Expert assumption on mass reduction due to advancement in manufacturing and assembly methods and improved material characteristics [35].
Gas turbine Mass	+17 %	Change of engine architecture from 3-spool to geared turbofan: integration of heavy gearbox, two stage HPT, fast running LPT with less stages
Gas turbine Performance	+4.4 %	Increased temperature and pressure levels of thermodynamic cycle, improved component efficiencies, slightly higher bypass ratio at constant engine diameter
Aerodynamic Performance	+11 %	Adopting the aerodynamic performance reference aircraft obtained by Streit et al. [34]

3.3 HLFC Aircraft

This chapter examines the HLFC aircraft in detail and compares it to the baseline aircraft discussed earlier. As the HLFC aircraft is the main focus of this study, a detailed examination is warranted. This includes a comprehensive examination of various facets such as geometric modifications, aerodynamic considerations, mass considerations, system integration and engine-related changes. By exploring these elements, it is hoped to gain a thorough understanding of the complexities that differentiate the HLFC aircraft from its baseline counterpart.

For the design of the aircraft with the HLFC system, a step-by-step integration of the technologies was carried out. This methodical approach was used to systematically evaluate the impact of each component, allowing a thorough examination of their effects in isolation. The process also aimed to identify potential design drivers that could have a significant impact on the overall performance and efficiency of the aircraft.

3.3.1 Geometry

The design of the HLFC wing was based on the specifications of the AIRBUS XRF1 aircraft, as detailed in Chapter 3.1. Figure 10 shows a perspective view of the HLFC aircraft, the basis for CFD calculations and far-field drag analysis. For the shape design, a cruise flight condition with $M_\infty = 0.83$, $C_L = 0.5$ and a flight altitude of 36 000 ft was considered. Off-design scenarios were also investigated, including a variation of M_∞ (0.83 ± 0.02), C_L (0.5 ± 0.05) and flight altitude (36 000 ft $\pm$ 3000 ft), resulting in a total of 9 different flow conditions. In terms of wing shape modifications, the changes were limited to the outer wing, outboard of the engine position (see Figure 10, shaded area in red). The wing thickness remained unchanged in order to maintain the necessary fuel volume and avoid detrimental effects on the wing's structural integrity. The leading edge incorporated 4 HLFC suction panels, each with an individual length of 5 m (see Figure 10, shaded area in green). The segment length was limited due to maintenance and handling considerations. The wing geometry for the current study was derived from this shape design optimization, as described by Streit et al. [34]. In particular, modifications were made to the airfoils to optimize laminar flow conditions over the wing surface.

3.3.2 Aerodynamics

Subsequently, the ADE is calibrated to match the aerodynamic performance provided by the findings from Streit et al. [34]. Table 6 lists the aerodynamic performance without the horizontal tail plane (HTP) at cruise flight condition of the baseline and the HLFC aircraft. It shows a L/D ratio of 20.5 for the baseline and is compared to the other configurations. When changing from the baseline

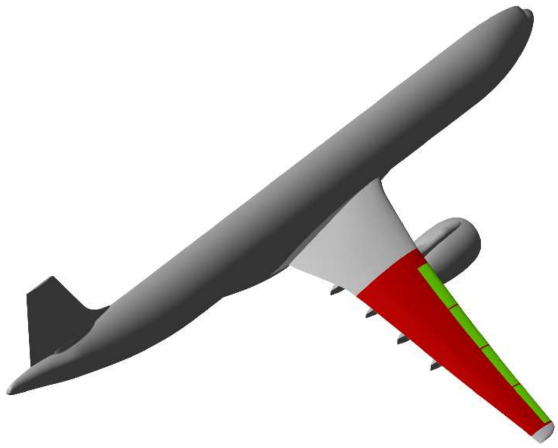

Figure 10 – Depiction of the HLFC outer wing (red) and leading-edge suction panels (green) [34].

to the HLFC aircraft, two things can be observed. First, the HLFC aircraft with a fully turbulent outer flow (e.g. the HLFC system not operating) reduces the aerodynamic performance by 1.1 %, mainly due to the increase in wave drag, inherent to HLFC airfoils at high Mach numbers. Once the HLFC system is turned on, the wing friction drag is reduced together with the viscous pressure drag. In order to have a more realistic model of the aerodynamics, the details of the suction segments were considered. The suction area was adjusted to the actual extent of the suction surface, which results in turbulent wedges originating from the spanwise interface between suction panels (see Figure 11). This results in a L/D ratio of 21.2 for the HLFC aircraft with wedges and thus, an increase in aerodynamic performance by 3.5 %. Note, that the detrimental effect of turbulent wedges at suction segment boundaries is a merely integrational aspect and depends in magnitude on design specifics, such as chordwise laminar extent, number of suction segments and segment interface layout.

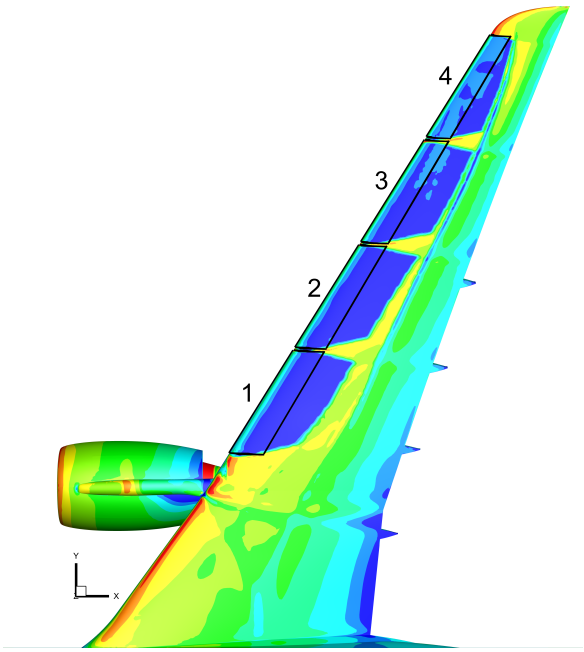

Figure 11 – Skin friction coefficient for the HLFC wing's upper side. Laminar areas coloured blue [36].

3.3.3 Mass

To fully assess the performance of the HLFC system, it is necessary to integrate the HLFC technology into a more realistic aircraft model that takes into account all relevant factors. This requires a holistic approach that considers the impact of the HLFC system on the entire aircraft. To account for

Table 6 – Aerodynamic performance comparison between the baseline and HLFC aircraft configuration (without HTP) at cruise flight condition (M_∞ = 0.83, $C_L \approx 0.5$, flight altitude of 36 000 ft).

Configuration	**Transition**	**L/D** [-]	**ΔL/D (to Baseline)** [%]
Baseline	**Fully Turbulen**t	**20.5**	**0.0**
HLFC Aircraft	Fully Turbulent	20.2	-1.1
HLFC Aircraft	Laminar / Turbulent (HLFC System)	21.3	+4.1
HLFC Aircraft	Laminar / Turbulent (HLFC System + Wedges)	21.2	+3.5

the changes in the wing assembly resulting from the integration of the HLFC system, an upscaling strategy is used, as introduced by van de Kamp et al. [12]. This strategy involves a linear extrapolation of the geometry and laminate thickness of the outer-wing. Assuming that the changes introduced by the HLFC system are relatively small, this approach provides a rough estimate of the outer wing mass distribution. The outer wing is simply tapered and a homogeneous laminate thickness distribution is assumed, with no areas of massive local load introduction such as landing gear or pylon attachments. However, a more detailed wing design would be required to reduce the uncertainties. Overall, the integration of the HLFC system into a realistic aircraft model using an upscaling strategy is crucial to assess the effectiveness of the technology at a holistic aircraft level.
For the estimation of the complete HLFC wing, some additional assumptions had to be made compared to the upscaling strategy by van de Kamp et al. [12] in order to arrive at the total wing mass. Table 7 provides an overview of the total wing mass breakdown and the change from the baseline to the HLFC aircraft. Since the design and mass estimation of the ribs is highly complex and depends not only on the wing loading but also on the landing gear or pylon attachments, the rib mass is assumed to be equal to the baseline mass and is therefore not changed. For the other components of the wing box, the upscaling strategy is used. In addition, the fixed leading edge component is split into the leading edge structure and the suction glove, which represents the microperforated titanium skin. The leading edge structure is scaled according to the upscaling strategy, while the suction glove is added to the HLFC aircraft model. The movable leading edge was changed from a slat system to the Kruger flap high-lift system. The evaluation of the Kruger flap system was critical to the assessment as it is a new system introduced to the HLFC aircraft. In this work a Torenbeek method [37] is applied to estimate the mass of the Kruger flap system. The Kruger flap mass is estimated by

$$m_{Kruger} = \frac{220}{g} \cdot S_{Kruger} \cdot f_{Calibration} \, , \tag{5}$$

with a constant specific weight divided by the gravity g, as well as the planform area S_{Kruger} of the Kruger flap in the retracted position and a calibration factor. The calibration factor is obtained from the reference aircraft design and is used to estimate the Kruger flap mass. The results show that the mass of the total movable leading edge is very similar to the baseline. As the other components remain unchanged with respect to the HLFC system, a total wing mass increase of 941 kg is estimated.

3.3.4 Systems

The next step is to install the rib-integrated compressors. To maintain laminarity on the upper surface of the outer wing, the compressors are used to partially suck in the airflow, which reduces the friction drag on the wing. The compressors ensure a negative pressure gradient between the ambient air on the suction surface and the sealed chambers inside the leading edge. An external company, Safran Cabin, with experience in the design and certification of compressors used in civil aviation, performed a preliminary design of a suitable compressor model according to the specifications. In general, the suction area spans 20 m of the outer wing, which is divided into four equally spaced

Table 7 – Wing mass breakdown estimation from the Baseline to HLFC Aircraft in kg.

Component		Baseline			HLFC Aircraft			Diff.
		Full Wing	Half Wing	Outer Wing (LE + WB)	Outer Wing (LE + WB)	Half Wing	Full Wing	
Ribs		3010.0	-	-	-	-	3010.0	±0.0
Shell		13096.0	6548.0	1735.2	1865.2	6678.0	13355.9	+260.0
Spars		3157.0	1578.5	418.3	428.2	1588.4	3176.7	+19.7
Misc.		0.0	0.0	0.0	56.9	56.9	113.7	+113.7
Wing Box (WB)	Σ	19263.0	9631.5	2552.3	2749.0	9828.2	19656.4	+393.4
Structure		1193.0	596.5	158.1	267.0	705.4	1410.8	+217.8
Suction Glove		0.0	0.0	0.0	171.7	171.7	343.4	+343.4
Fixed Leading Edge	Σ	1193.0	596.5	158.1	438.7	877.1	1754.2	+561.2
Fixed Trailing Edge	Σ	2243.0	-	-	-	-	2243.0	±0.0
Slat 1		447.3	-	-	-	-	447.3	±0.0
Outer Wing Slat 2-7		766.0	383.0	383.0	0.0	0.0	0.0	-766.0
Outer Wing Kruger 1-8		0.0	0.0	0.0	375.8	375.8	751.5	+751.5
Movable Leading Edge	Σ	1213.3	606.7	383.0	375.8	599.4	1198.8	-14.5
Flaps		1266.0	-	-	-	-	1266.0	±0.0
Aileron		282.0	-	-	-	-	282.0	±0.0
Spoilers		245.0	-	-	-	-	245.0	±0.0
Movable Trailing Edge	Σ	1793.0	-	-	-	-	1793.0	±0.0
Pylon Attachments	Σ	420.0	-	-	-	-	420.0	±0.0
Landing Gear Support	Σ	971.0	-	-	-	-	971.0	±0.0
Miscellaneous	Σ	667.0	-	-	-	-	667.0	±0.0
Total Wing	Σ	27762.0	13881.0	3181.8	3651.8	14351.7	28703.4	+941.4

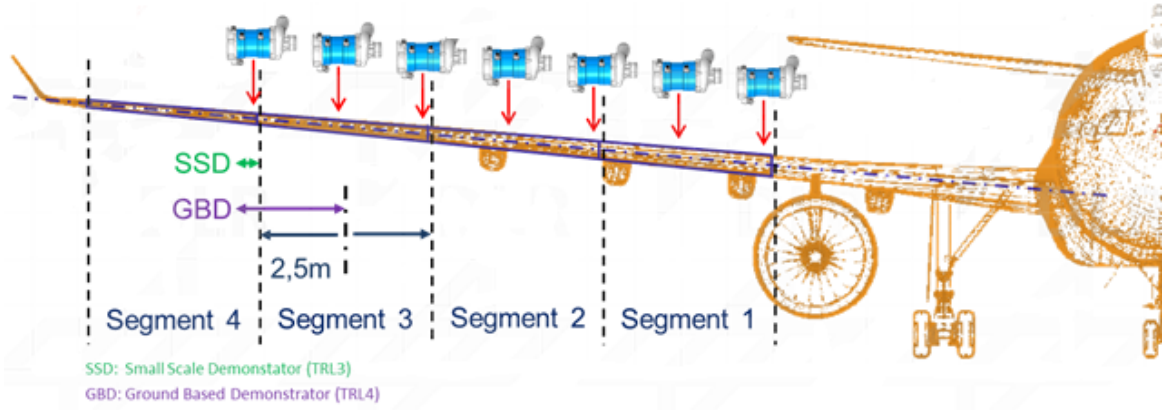

Figure 12 – Rib-integrated compressors to provide suction for the HLFC system [12].

segments, as shown in Figure 12. The mass flow of each compressor has been estimated from the aerodynamic requirements and is described in more detail in [34]. According to the compressor designed by Safran Cabin, the expected mass is up to 11.4 kg per unit (compressor and attached inverter). However, additional mounting elements have to be taken into account and an additional margin of 10 % is assumed, resulting in a total of 13 kg per unit. Therefore, the sum of the seven compressors per half span results in an additional mass of 176 kg.

In addition to the development of the HLFC system, another system component has been replaced. The WIPS (Wing Ice Protection System), as the name suggests, is used to protect the wing from ice build-up, which can lead to a degradation of aerodynamic lift and a disturbance of laminar flow. The most common conditions that require the use of WIPS include flying through clouds with temperatures at or below freezing, flying in visible moisture such as rain or snow, or flying in high humidity areas where supercooled water droplets may be present. In order to allow for a proper system design, the certification regulations clearly define the icing conditions that need to be covered. WIPS functionality is conventionally provided by the bleed air system, but an inductive WIPS (iWIPS) has been introduced due to the limited space available in the leading edge. Furthermore, the use of a non-contact induction-based heating system provides an efficient maintenance approach by being implemented on independent, individually replaceable modules. From [12], the mass of the iWIPS

is estimated by the coil structure shown in Figure 13. A coil contains 60 wires with a cross-section of 4 mm^2 and a material density of 8.69 mg/mm^3 for copper. With an additional margin of 20 % and the inverter, a mass of 50 kg is estimated for a 5 m segment with 3 coils. For the complete wing, two segments are heated on each side, giving a total system mass of 200 kg.

Figure 13 – Possible double layer installation of the coils system (shaded in orange and yellow).

3.3.5 Engine

The HLFC system and WIPS require electrical power to operate. HLFC systems also add mass to the overall configuration leading to changes in thrust requirements. The resulting demand must be provided by the engine and has implications for its design and fuel consumption. Consideration of the changes in engine requirements is critical in assessing overall system performance. The HLFC system not only introduces a mass penalty due to the change in wing assembly and additional system components such as the rib-integrated compressors, but also increases the power requirement of the engines to drive the compressors as mentioned in Chapter 2.2.2. In addition, the change from a bleed air operated WIPS to an electric iWIPS, which requires shaft power take-off instead of bleed air, changes the engine power requirement.

The power requirements of the iWIPS depend on the weather conditions or the operating condition of the aircraft. Typically, a WIPS is active at lower altitudes up to approximately 25 000 ft. Above this altitude, the air is generally too dry for ice to form on the wings, and the use of the WIPS is not necessary. The power requirement of the iWIPS at aircraft level is estimated to be 100 kW to 120 kW depending on the atmospheric conditions. For the purpose of this study and comparability between the baseline and the HLFC aircraft, the design case with a shaft power take-off of 120 kW is used. For simplicity, it is assumed that iWIPS is active during the take-off, climb, descent and approach & landing segments and is only deactivated during the cruise segment.

Therefore, the engine design requirements for HLFC aircraft have changed from bleed air to more shaft power take-off, but the thrust requirements have also changed due to the change in aircraft mass, while the thrust-to-weight ratio remains constant. Table 8 provides an overview of the required engine off-takes for the baseline configuration and different operating conditions. An engine design is derived for the HLFC configuration and performance maps for all relevant off-take scenarios are provided.

Table 8 – Engine offtakes overview for different operating conditions and engine settings

Description	**Deck ID**	**Offtakes**		**Altitude**		**Mach Number**		
		Shaft-Power [kW]	**Bleed Air [kg/s]**	**Min. [FL]**	**Max. [FL]**	**Min. [-]**	**Max. [-]**	**Add. [-]**
Baseline	MTO	255	2.901	0	300	0	0.6	-
	MCL	105	1.16	0	430	0	0.86	0.81, 0.83
Baseline + iWIPS	MTO	345	1.2	0	300	0	0.6	-
	MCL	225	1.16	0	430	0	0.86	0.81, 0.83
Baseline + HLFC	MCL	231	1.16	300	430	-	-	0.81
	MCL	216	1.16	300	430	-	-	0.83
	MCL	217	1.16	300	430	-	-	0.85

4 Results

This chapter presents the key findings of the investigation of the HLFC system as applied to long-haul aircraft. The results are divided into two related sub-chapters: The Mission Performance Assessment and the Lifecycle Performance Assessment. The Mission Performance Assessment examines the overall aircraft performance and quantifies the impact of HLFC integration on fuel efficiency in different mission scenarios. It provides a realistic assessment of the technology's potential, taking into account mission-specific variables and expected degradation over time. At the same time, the lifecycle performance assessment considers the long-term economics of HLFC integration. By analysing three different scenarios, it examines the technology's impact on the total cost of ownership, including factors such as maintenance, fuel efficiency, and operating costs.

4.1 Mission Performance Assessment

Once the stepwise integration of the new technology is established, a detailed assessment of the HLFC system can be performed. Figure 14 shows the result of this incremental integration, starting from the baseline and ending with the HLFC aircraft. Starting from the baseline, the wing planform and aerodynamics are adjusted. This adjustment resulted in the maximum potential improvement in aircraft performance of the HLFC system with a 4.6 % reduction in block fuel. However, the integration of the system into the aircraft reduces this maximum potential improvement.

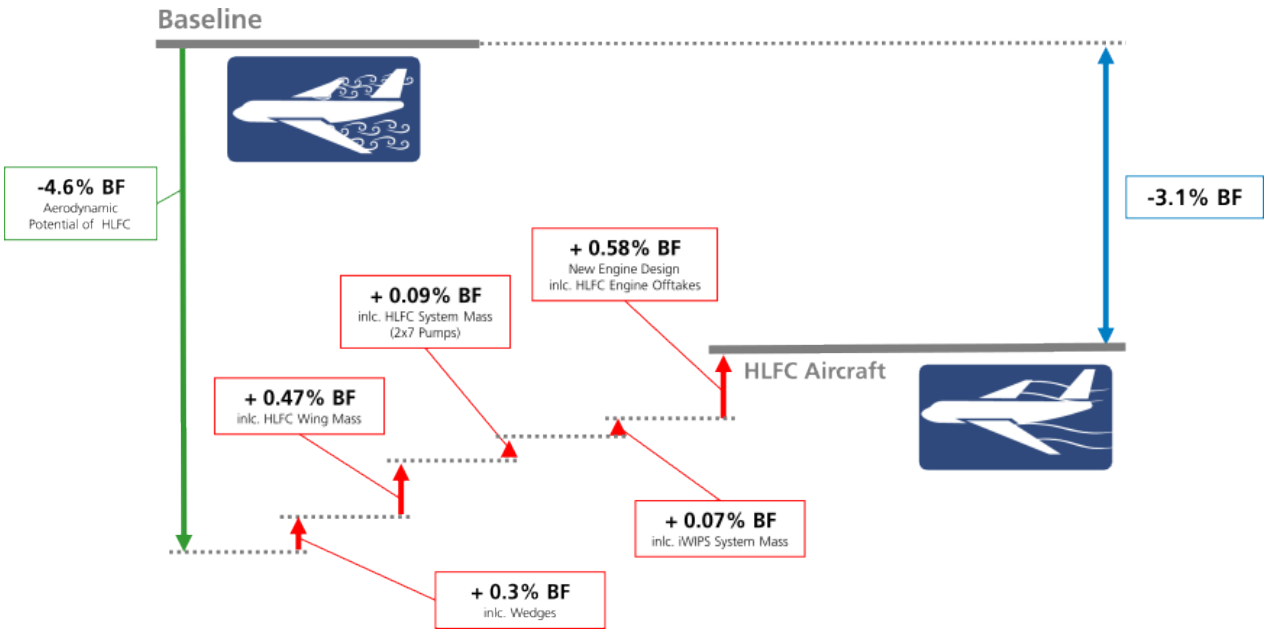

Figure 14 – Ladder chart: Block fuel breakdown from Baseline to HLFC Aircraft.

Firstly, the aerodynamic data given in Table 6 were used to carefully calibrate the aerodynamic polar. A comparative analysis between the baseline aircraft and the HLFC aircraft shows a decrease in aerodynamic performance, which can be attributed to the transition from a turbulent wing geometry (baseline aircraft) to a laminar wing geometry (HLFC aircraft without HLFC operation). However, the introduction of the HLFC system immediately restored the aerodynamic performance to a higher performance level. Figure 15 shows the breakdown of the aircraft drag components in comparison with the baseline. The analysis highlights two primary contributors to the total drag: the wing frictional and viscous pressure drag, and the induced drag. The primary objective of this work revolves around the reduction of wing viscous drag, and a notable reduction of about 25 % is observed in the transition from the turbulent baseline aircraft to the HLFC aircraft. Despite the observed aerodynamic improvements in viscous drag, there is an associated drag penalty in wave drag for the HLFC wing. Especially for laminar airfoils, the wave drag is more prominent compared to turbulent airfoils, resulting from the required acceleration on the suction side to allow for continuous damping of boundary layer instabilities downstream of the suction region. However, due to the small absolute value of wave drag, this can be compensated by greater savings through the laminarization. To have a more

realistic assessment of the aerodynamics, the turbulent wedges created between the suction panels on the wing are included, which marginally reduces the aircraft performance by 0.3 %. The remaining drag components remain constant as they have not been modified within the scope of this work.

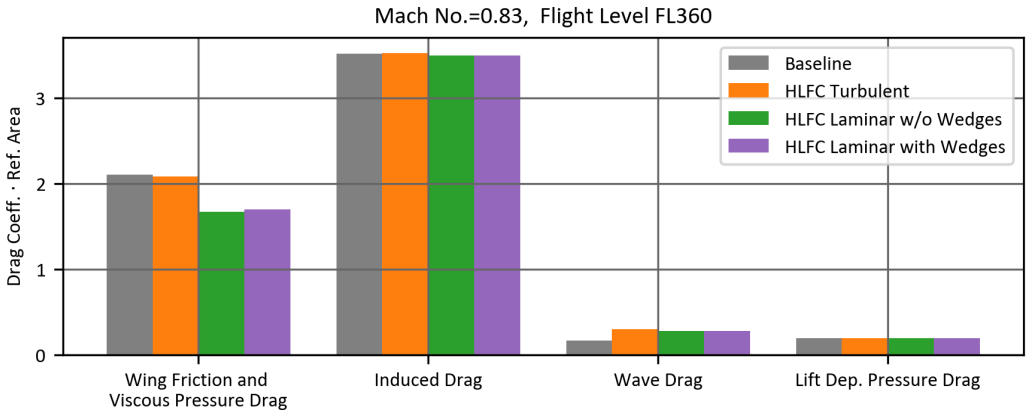

Figure 15 – Relative change of main drag components compared to the baseline aircraft [34].

Secondly, the additional mass due to the HLFC system has to be taken into account. This was done by estimating a new wing mass, integrating the HLFC compressors and the iWIPS system mass (see Chapter 3.3.3). It is worth noting that the remaining structural elements of the airframe have not been modified, and the same technological assumptions have been maintained as for the baseline aircraft. These additional masses due to the HLFC system resulted in a slightly higher OEM compared to the baseline aircraft, mainly driven by increases in both the wing box mass and the fixed leading-edge mass. Consequently, this additional mass has resulted in a reduction in overall performance of 0.63 %, as shown in Figure 14.
Finally, the change in engine offtakes must be considered. The HLFC system requires shaft power to operate the HLFC compressors. In addition, the iWIPS was integrated, which used shaft power instead of bleed air as a conventional WIPS. A redesign of the engine incorporating the changes in engine offtake leads to an overall reduction in aircraft performance of 0.58 %.
All these aspects together resulted in an overall improvement of 3.1 % with the integration of an HLFC system and revealed two key findings that adversely affect the performance of the HLFC system: the increased wing mass and the incorporation of additional engine offtakes. Particularly, the estimation of wing mass is subject to high uncertainty due to the implementation of a top-down approach. Given the inherent complexity of the wing component, adopting high-fidelity methods would yield deeper insights and potential improvements. Considering that the integration of the HLFC system was executed through a retrofit design approach without any modifications to the planform or engine nacelle diameter, further enhancements to the design are possible. Maintaining a constant outer diameter for the engine nacelle was crucial in order to preserve the aerodynamics of the wing with HLFC. Consequently, a comprehensive multidisciplinary optimization encompassing the wing (including planform, aerodynamics, and mass) and the engine (such as bypass ratio and offtakes for the HLFC system) holds the potential for additional performance benefits.
In order to have a comprehensive comparison between the baseline and the HLFC aircraft, the key aircraft characteristics are listed in Table 9. The results indicate a slightly higher structural mass for the HLFC aircraft, with a 1.1 % increase in OEM. However, due to the improved aerodynamics achieved through the HLFC system, the MTOM remains relatively comparable. The mission performance analysis demonstrates improvements in terms of block fuel consumption for both the design mission and the study mission, with reductions of 3.1 % and 2.7 % respectively. This leads to corresponding improvements in fuel efficiency and a reduction in CO2 emissions, as these are directly related to the reduction in block fuel consumption.

4.2 Lifecycle Performance Assessment

This Chapter deals with the results of the comparative lifecycle simulation. Hereby, the outputs of the HLFC aircraft are directly compared to those of the baseline. Each scenario is compared to itself, i.e.

Table 9 – Comparison of the key characteristics of the baseline and HLFC aircraft.

Parameter	Unit	Baseline	HLFC Aircraft
Key Sizing Parameters			
W/S = MTOM / Wing Ref. Area	kg/m2	599.5	598.6
T/W = SLST / MTOM	-	0.296	0.296
Design Masses			
MTOM	t	224.55	223.93
MLM	t	181.99	182.95
MZFM	t	172.26	173.59
OEM	t	124.26	125.59
Design Mission Performance			
Block Fuel	t	61.0	59.2
TSFC (average cruise)	g/s/kN	14.69	14.79
Lift-to-drag-ratio (average cruise)	-	19.41	20.3
Fuel Efficiency	L/PAX/100km	2.55	2.47
CO2 Emissions	g/PAX/100km	6.29	6.1
Study Mission Performance			
Block Fuel	t	31.1	30.2
TSFC (average cruise)	g/s/kN	14.77	14.92
Lift-to-drag-ratio (average cruise)	-	19.15	20.1
Fuel Efficiency	L/PAX/100km	2.38	2.31
CO2 Emissions	g/PAX/100km	5.87	5.71

the “neutral” scenario simulation of the HLFC aircraft is compared to the “neutral” scenario simulation of the baseline aircraft.

The fuel efficiency improvements, here depicted as relative block fuel changes, are shown in Figure 16, with the disadvantageous scenario in the left column, the neutral scenario in the centre, and the advantageous scenario in the right column. The block fuel savings potential ranges from 1.6 to 2.4 % on average, but can reach values up to 3.46 %. This value is slightly better than the previously mentioned 3.07 % from Figure 14 due to the fact that the Mach number variation, which was considered here, can be beneficial for the laminarity (see Figure 4 and Mach numbers > 0.83). While the majority of the expected changes in block fuel are negative (i.e. show that the HLFC aircraft burns less fuel than the baseline), there is a noticeable number of flights where this is not the case. However, the ratios of flights where the HLFC aircraft is more fuel efficient are 94 %, 95 %, and 96 % for the disadvantageous, neutral, and advantageous scenario, respectively. Generally, it should be noted that the distribution of the Δblock fuel values (top plots) is favourable for the HLFC aircraft, i.e. the majority of fuel savings are high (2 % and more).

The final set of results is shown in Figure 17. The top left plot depicts the overall economic impact, represented as ΔCDOC, while the breakdown into Δmaintenance cost, Δfuel cost, and Δcapital cost is shown in the bottom left, top right, and bottom right plot. In each, each scenario is shown as its own bar.

The ΔCDOC shows that the disadvantageous scenario leads to the HLFC aircraft being economically inferior to the baseline, i.e. an operator has to expect about 0.74 % higher cost when operating the laminar aircraft. This is not only due to the fact that the block fuel savings are lower in this scenario, but also because the fuel price is low (which limits the saved fuel cost to 4 million USD, see top right plot), the expected maintenance costs are high (about 7 million USD, bottom left) and the expected price increase is high (2.3 million USD, bottom right). In the neutral scenario, both aircraft have a relatively equal economic performance, as the fuel cost savings are outweighed by the increase in maintenance cost and capital cost. The advantageous scenario shows that up to 14.4 million USD can be saved, which is about 1 % of the CDOC. This is mostly due to the high fuel price development in this scenario, but is also affected by the low maintenance and capital cost. Generally, comparing the different bars within a plot shows that the fuel price aspect plays a significantly larger role than

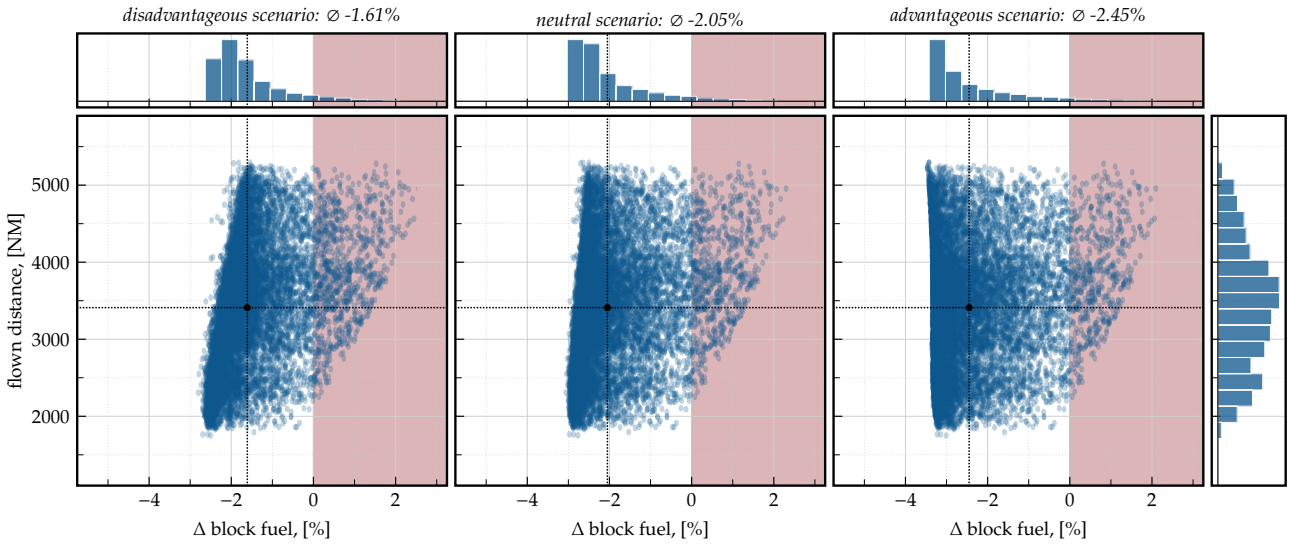

Figure 16 – Block fuel savings and flown distances for each scenario.

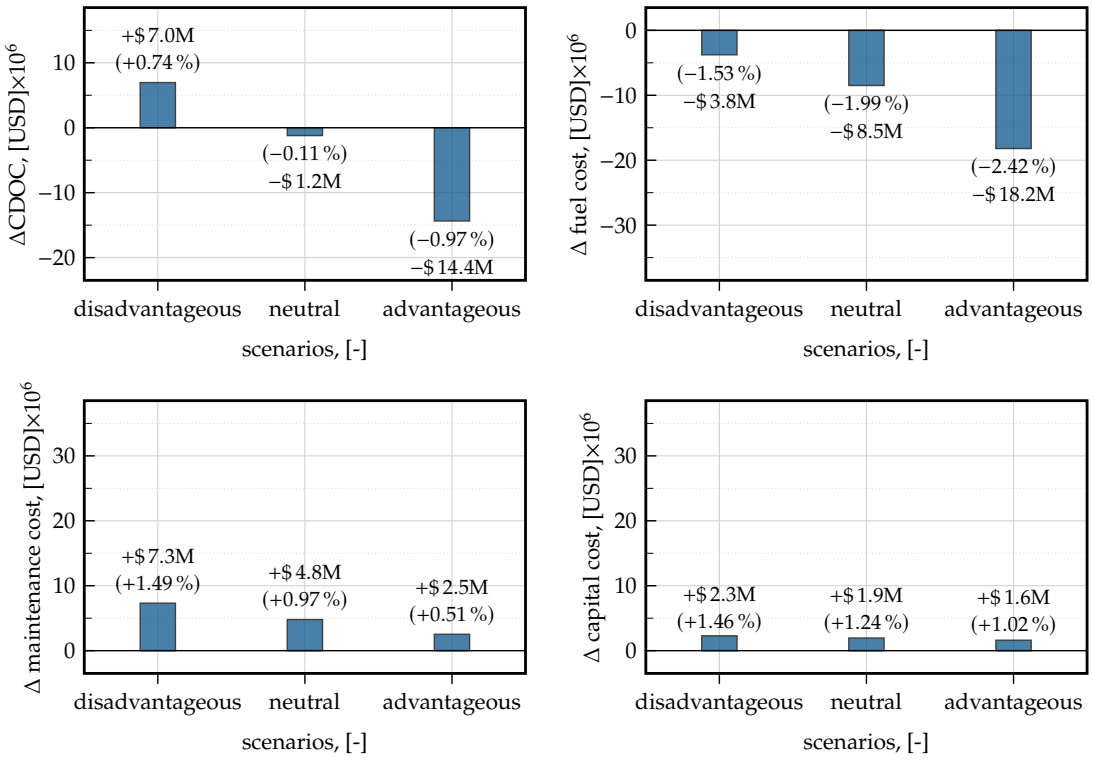

Figure 17 – Economic Comparison between the HLFC aircraft and the Baseline.

the maintenance and capital cost increase. This indicates that the fuel price uncertainty, which is impossible to predict for the next two decades, has the highest influence on the overall outcome.

5 Conclusion

In conclusion, the research conducted as part of the European Clean Sky 2 project HLFC-Win and the underlying design work has demonstrated the feasibility of integrating a HLFC system into the complex environment of an outer wing leading edge in an industrial context. This paper focused on a scientifically sound comparison between an aircraft equipped with HLFC and an aircraft of the same technology level without HLFC, considering various factors such as changes in geometry, mass, aerodynamics, and engine offtakes.

The mission-based performance assessment revealed a significant fuel efficiency improvement of over 3.1 % for the design mission, which translates into an average reduction in fuel consumption of

1.6 to 2.5 % when considering realistic route scenarios and expected degradation. This highlights the potential of HLFC technology to significantly improve overall aircraft performance and reduce environmental impact, especially in the context of expected fuel price increases. In addition, the three-scenario lifecycle simulation provided a comprehensive economic assessment. The results showed a scenario-dependent impact on total costs, ranging from a 0.7 % increase in an unfavorable scenario to a nearly 1 % reduction in a favorable scenario. The latter represents a significant cost saving of 15 million USD per HLFC aircraft over its lifetime. These results underscore the economic viability of HLFC technology and demonstrate its potential to not only improve aerodynamic and fuel efficiency, but also to generate significant cost savings for the aviation industry.
The potential to reduce drag has been limited by the design constraints of retrofitting the wing. A further significant increase in efficiency can be expected by incorporating laminar technologies from the beginning of the aircraft design process. This would involve adjustments to the wing planform and airfoil redesign, as well as multidisciplinary optimization of the wing aerodynamics, structural design, and systems design. In addition, the inner wing was not laminarized in this study due to high Reynolds numbers and complex flow topology. However, incorporating these considerations into new designs could further enhance aircraft efficiency and the efficacy of the laminar flow technologies.

Contact Author Email Address

Benjamin Fröhler
German Aerospace Center (DLR)
Institute of System Architectures in Aeronautics, Hamburg, Germany
mailto: benjamin.froehler@dlr.de

Copyright Statement

Acknowledgements

The project leading to this application has received funding from the Clean Sky 2 Joint Undertaking under the European Union's Horizon 2020 research and innovation program under grant agreement No: CS2-LPA-GAM-2020-2023-01.

Disclaimer

List of Abbreviations

ADE	Aircraft Design Environment
AEO	Annual Energy Outlook
CDOC	Cumulative DOC
DOCs	Direct Operating Costs
EIS	Entry-Into-Service
FC	Flight Cycle
FH	Flight Hour

FL	Flight Level
HLFC	Hybrid Laminar Flow Control
HTP	Horizontal Tail Plane
ICA	Initial Cruise Altitude
ISA	International Standard Atmosphere
iWIPS	Inductive Wing Ice Protection System
LE	Leading Edge
Ma	Mach number
MMO	Max. operating Mach number
MLM	Maximum Landing Mass
MTOM	Maximum Take-Off Mass
OEM	Operating Empty Mass
PAX	Passenger
RWY	Runway
SL	Sea Level
SLST	Sea Level Static Thrust
SMEs	Subject Matter Experts
TLARs	Top-Level Aircraft Requirements
TSFC	Thrust Specific Fuel Consumption
WIPS	Wing Ice Protection System

References

[1] European Commission. *Flightplan 2050: Europe's Vision for Aviation; Maintaining Global Leadership and Serving Society's needs; Report of the High-Level Group on Aviation Research*. policy. Publ. Off. of the Europ. Union, Luxembourg, 2011.

[2] Collier F.S. An overview of recent subsonic laminar flow control flight experiments. In *23rd Fluid Dynamics, Plasmadynamics, and Lasers Conference*, 2012.

[3] Joslin R.D. Overview of laminar flow control. Nasa technical publication nasa/tp-1998-208705, NASA Center for AeroSpace Information (CASI), 1998.

[4] Maddalon D.V and Braslow A.L. Simulated-airline-service flight tests of laminar-flow control with perforated-surface suction system. Nasa technical paper 2966, NASA Langley Research Center Hampton, 1990.

[5] Maddalon D.V, Collier F.S, Montoya L.C, and Putnam R.J. *Transition Flight Experiments on a Swept Wing with Suction*, pages 53–62. Springer Berlin Heidelberg, 1989.

[6] Maddalon D.V and Wagner R.D. Boeing 757 hybrid laminar-flow control flight tests. *Langley Aerospace Test Highlights, NASA TM-104090*, 159, 1990.

[7] Maddalon D.V. Hybrid laminar-flow control flight research. *Research and Technology, NASA, TM*, 4331:47, 1991.

[8] Henke R. "A 320 HLF Fin" flight tests completed. *Air & Space Europe*, 1(2):76–79, March 1999.

[9] Redeker G., Quast A., and Thibert J.J. Das A320 Laminar-Seitenleitwerks-Programm. *Deutsche Gesellschaft für Luft- und Raumfahrt - Lilienthal-Oberth e.V.*, JAHRBUCH 1992 Vol. III:1259–1270, September 1992.

[10] Kilian T. and Horn M. Verification of a chamberless HLFC design with an outer skin of variable porosity. *CEAS Aeronautical Journal*, 12(4):835–845, August 2021.

[11] van de Kamp B. and Ropte S. Innovation report 2021: Technologies for sustainable aviation – the HLFC-WIN small scale demonstrator. Technical report, German Aerospace Center (DLR): Institute of Composite Structures and Adaptive Systems, 2021.

[12] van de Kamp B., Kleineberg M., and Schröder A. Hybrid laminar flow control ready for series application. *Proceedings of the Aerospace Europe Conference - EUCASS - CEAS - 2023*, 2023.

[13] Fröhler B.M.H.J, Häßy J., and Abu-Zurayk M. Development of a medium/long-haul reference aircraft. *CEAS Aeronautical Journal*, 14(3):693–713, may 2023.

[14] Seider D., Fischer P.M, Litz M., Schreiber A., and Gerndt A. Open source software framework for applications in aeronautics and space. In *2012 IEEE Aerospace Conference*. IEEE, mar 2012.

[15] Boden B., Flink J., Mischke R., Schaffert K., Weinert A., Wohlan A., and Schreiber A. RCE, 2019.

[16] Boden B., Flink J., Först N., Mischke R., Schaffert K., Weinert A., Wohlan A., and Schreiber A. RCE: An integration environment for engineering and science. *SoftwareX*, 15:100759, July 2021.

[17] Alder M., Moerland E., Jepsen J., and Nagel B. Recent advances in establishing a common language for aircraft design with CPACS. In *Aerospace Europe Conference 2020*, 2020.

[18] Wöhler S., Atanasov G., Silberhorn D., Fröhler B., and Zill T. Preliminary aircraft design within a multidisciplinary and multifidelity design environment. *Aerospace Europe Conference 2020*, 2020.

[19] Silberhorn D. AMC – Aircraft Mission Calculator: Documentation. Technical report, Deutsches Zentrum für Luft- und Raumfahrt e.V, 2020.

[20] Pohya A.A, Wehrspohn J., Meissner R., and Wicke K. A modular framework for the life cycle based evaluation of aircraft technologies, maintenance strategies, and operational decision making using discrete event simulation. *Aerospace*, 8(7):187, jul 2021.

[21] Clark P. *Buying the Big Jets : Fleet Planning for Airlines*. Routledge, an imprint of the Taylor & Francis Group, Abingdon, Oxon New York, NY, 3 edition, 2017.

[22] Suwondo E. *LCC-OPS : Life Cycle Cost Application in Aircraft Operations*. PhD thesis, TU Delft, Bandung, 2007.

[23] Aircraft Commerce. Owners and operators guide: A330-200/-300. *The Journal for Commercial Aircraft Business*, April 2008.

[24] Aircraft Commerce. Owners and operators guide: Rolls-royce trent family. *The Journal for Commercial Aircraft Business*, August 2012.

[25] Pohya A.A, Wicke K., and Kilian T. Introducing variance-based global sensitivity analysis for uncertainty enabled operational and economic aircraft technology assessment. *Aerospace Science and Technology*, 122:107441, February 2022.

[26] Young T. *Investigations into the Operational Effectiveness of Hybrid Laminar Flow Control Aircraft*. PhD thesis, Cranfield University, Cranfield, UK, 2002.

[27] Flightradar24. Flight history for aircraft D-AIKI. `https://www.flightradar24.com/data/aircraft/d-aiki`, December 2019. last accessed on 2021-01-11.

[28] Hersbach H., Bell B., Berrisford P., Biavati G., Horányi A., Muñoz Sabater J., Nicolas J., C. Peubey, Radu R., Rozum I., Schepers D., Simmons A., Soci C., Dee D., and Thépaut J.-N. ERA5 hourly data on pressure levels from 1979 to present, 2018. Copernicus Climate Change Service (C3S) Climate Data Store (CDS). Accessed on 03/01/2021.

[29] U.S. Department of Transportation, Bureau of Transport Statistics. T-100 segment data - all airlines - all airports. `https://www.transtats.bts.gov/Fields.asp?gnoyr_VQ=FMG`, 2021. last accessed on 2021-16-04.

[30] U.S. Department of Transportation, Energy Information Administration (EIA). Annual energy outlook 2022. table 12: Petroleum & other liquid prices. `https://www.eia.gov/outlooks/aeo/tables_side.php`, 2022. last accessed on 2022-03-17.

[31] Pohya A.A, Wicke K., and Wende G. Informed decision-making in aerospace technology assessments: Combining evidence theory and probability theory for epistemic and aleatory uncertainty quantification. *Aerospace Science and Technology*, 2024. submitted and under review.

[32] Görtz S., Abu-Zurayk M., Ilic C., Wunderlich T.F., Keye S., Schulze M., Kaiser C., Klimmek T., Süelözgen Ö., Kier T., Schuster A., Daehne S., Petsch M., Kohlgrüber D., Häßy J., Mischke R., Weinert A., Knechtges P., Gottfried S., Hartmann J., and Fröhler B. Overview of collaborative multi-fidelity multidisciplinary design optimization activities in the DLR project VicToria. In *AIAA AVIATION 2020 FORUM*. American Institute of Aeronautics and Astronautics, jun 2020.

[33] Bertram O. Neue Entwurfsmethoden zukünftiger Steuerflächenkonzepte: (im LuFo V-2 Con.Move-Verbundprojekt). Technical report, Deutsches Zentrum für Luft- und Raumfahrt e.V, 2020.

[34] Streit T., Kruse M., Kilian T., and Petropoulos I. Aerodynamic design and analysis of HLFC wings within the European project HLFC-WIN. In *33rd Congress of the International Council of the Aeronautical Sciences, ICAS 2022*, September 2022.

[35] Sinha K., Klimmek T., Schulze M., and Handojo V. Loads analysis and structural optimization of a high aspect ratio, composite wing aircraft. *CEAS Aeronautical Journal*, 12(2):233–243, feb 2021.

[36] Kilian T. and Schrauf G. HLFC technology integration on a long-range wing. In *Deutscher Luft- und Raumfahrtkongress 2023, Stuttgart*, 2023.

[37] Torenbeek E. *Advanced Aircraft Design: Conceptual Design, Technology and Optimization of Subsonic Civil Airplanes*. Wiley; 1. Edition, 2013.